

## Supporting Information

# Highly luminescent CuGa<sub>x</sub>In<sub>1-x</sub>S<sub>y</sub>Se<sub>2-y</sub> nanocrystals from organometallic single-source precursors

*Oliver Kluge<sup>1</sup>, Ilan Jen-La Plante<sup>1</sup>, Mahmud Diab<sup>1</sup>, Michael Volokh<sup>1</sup>, Ayelet Teitelboim<sup>2</sup>,  
Taleb Mokari<sup>1\*</sup>*

<sup>1</sup>Department of Chemistry and Ilse Katz Institute for Nanoscience and Nanotechnology, Ben-Gurion University of the Negev, Beer Sheva, Israel

<sup>2</sup>Department of Physics of Complex Systems, Weizmann Institute of Science, Rehovot, Israel

\*E-mail: mokari@bgu.ac.il

### **Influence of the solvent**

Mixtures of Trioctylamine (TOA) and Dodecanethiol (DDT) have been found to give the best results, regarding the homogeneity of the nanocrystalline product and the resulting photoluminescence quantum yields. The mixed solvent system is able to dissolve the precursor compounds at room temperature. Whereas Trioctylamine serves as a ligand and solvent during the synthesis only, DDT is also a source of sulfur and a capping ligand for the resulting particles. The temperature of 275 °C has been chosen by taking the bulk decomposition of the precursor compounds into account,<sup>1</sup> while avoiding superheating of DDT.

Regarding other common solvents for nanoparticle synthesis, for example the non-coordinating octadecene (90 % purity), the solubility of the precursor compounds is much lower at room temperature, resulting in multiple thermolysis products (Fig. S1). Since the product is obviously not homogenous in size, shape and possibly also composition of the nanocrystals, the thermolysis in octadecene has not been further investigated. Solutions of the precursor compounds in Oleylamine (70 % purity) are not stable at room temperature, *i.e.* they turn black during the dissolution process.

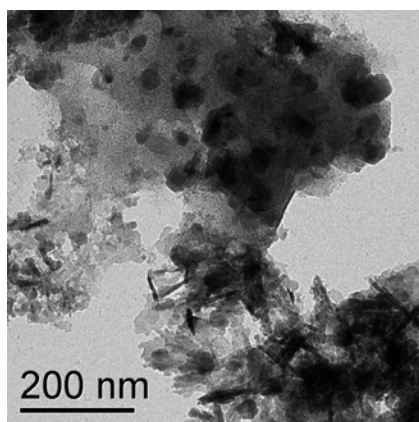


**Figure S1.** Inhomogeneous product obtained by heating precursor **1** to 250 °C in octadecene.

### **Wurtzite-structured contamination**

In the case of gallium-rich samples the nanocrystalline product is contaminated by a negligible amount of wurtzite-structured nanoribbon-shaped multinary material (Fig. S2).<sup>2,3</sup> This contamination can be easily removed by centrifugation of toluene solutions of the nanocrystal samples, as it is less soluble. With increasing ratio of DDT/TOA the fraction of the wurtzite structured contamination increases, emphasizing the necessity of TOA as additional ligand during the synthesis.

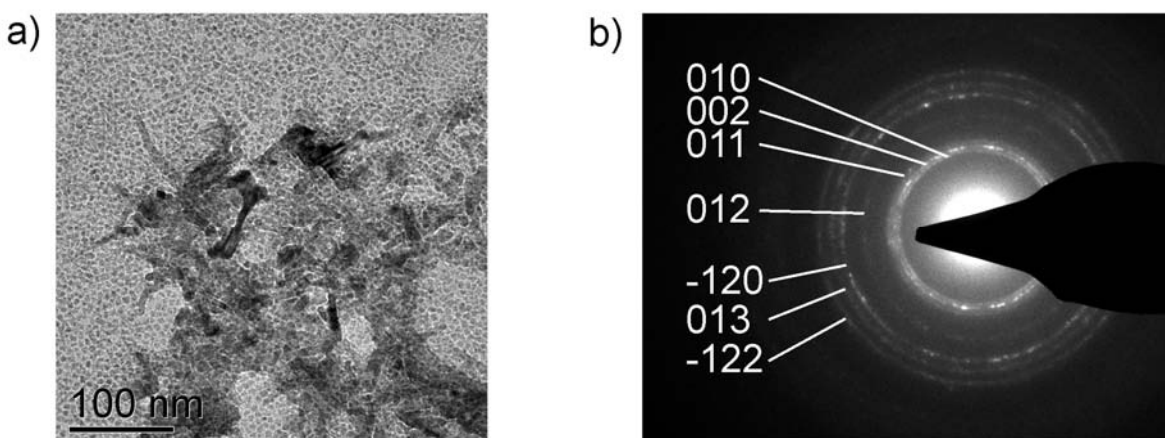


**Figure S2.** a) TEM image of wurtzite-CuGaS<sub>2</sub> nanoribbon contamination in a sample obtained from precursor **1** as described in the Experimental Section. b) Indexed SAED image of the wurtzite-CuGaS<sub>2</sub>.

### **EDX spectroscopy**

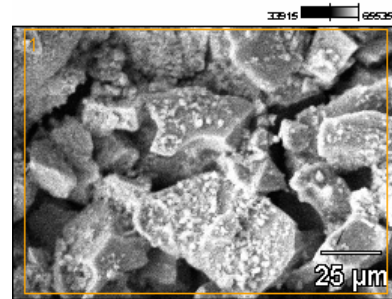


**Figure S3.** SEM image of a ZnS-passivated nanoparticle sample obtained with a precursor ratio (2 to 1+2) of 0.5. The rectangular area (marked orange) was used in EDX spectroscopy.

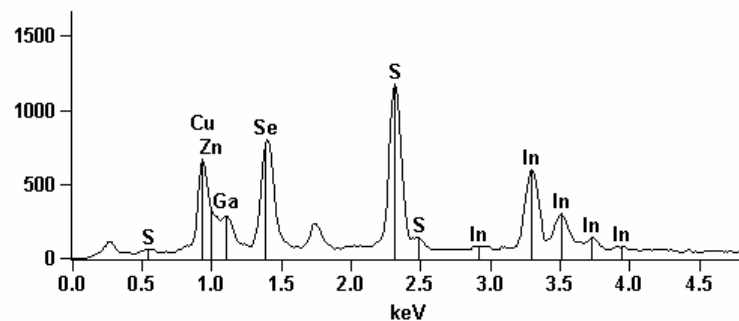


**Figure S4.** EDX spectrum of a ZnS-passivated nanoparticle sample obtained with a precursor ratio (2 to 1+2) of 0.5. Due to the strong overlap for the L lines of Cu, Zn and Ga, the line analysis was also performed with the respective K lines. Values found (at.%): Cu(K) 10.4+-0.7, Ga(K) 4.8+-0.5, In(L) 11.5+-0.5, S(K) 56.3+-0.6, Se(L) 11.6+-0.3, Zn(K) 5.5+-0.8; Cu(L) 14.8+-0.5, Ga(L) 12.1+-0.5, In(L) 8.1+-0.3, S(K) 42.9+-0.5, Se(K) 10.3+-0.3, Zn(L) 11.9+-0.5.

**Table S1.** EDX data (at.%) for the particles before surface-passivation with ZnS (compare Figure 2a in the article).

Ratio 1 to 2	EDX line analysis	Cu	error	Ga	error	In	error	S	error	Se	error
only 1	Cu(K), Ga(K), S(K)	21,3	0,5	24,1	0,9	-	-	54,6	0,4	-	-
	Cu(L), Ga(L), S(K)	21,0	0,3	26,4	0,5	-	-	52,6	0,4	-	-
5 to 1	Cu(K), Ga(K), In(L), S(K), Se(L)	11,2	0,5	11,1	0,4	5,4	0,3	66,8	0,4	5,6	0,2
	Cu(L), Ga(L), In(L), S(K), Se(L)	14,6	0,3	17,2	0,5	4,4	0,2	58,5	0,4	5,3	0,2
3 to 1	Cu(K), Ga(K), In(L), S(K), Se(L)	13,9	0,7	9,7	1,1	9,1	0,4	55,7	0,6	11,7	0,3
	Cu(L), Ga(L), In(L), S(K), Se(L)	20,2	0,5	19,1	0,4	6,6	0,3	43,6	0,5	10,5	0,3
2 to 1	Cu(K), Ga(K), In(L), S(K), Se(L)	17,3	0,5	12,9	0,8	8,3	0,3	53,1	0,4	8,4	0,3
	Cu(L), Ga(L), In(L), S(K), Se(L)	19,8	0,4	18,7	0,6	7,0	0,3	46,6	0,4	7,8	0,3
1 to 1	Cu(K), Ga(K), In(L), S(K), Se(L)	19,2	0,9	7,7	1,3	14,6	0,6	44,2	0,6	14,3	0,2
	Cu(L), Ga(L), In(L), S(K), Se(L)	23,0	0,7	15,1	0,5	11,8	0,4	37,1	0,5	13,0	0,2
1 to 2	Cu(K), Ga(K), In(L), S(K), Se(L)	20,0	0,8	7,5	1,0	16,3	0,5	41,0	0,5	15,1	0,4
	Cu(L), Ga(L), In(L), S(K), Se(L)	23,0	0,6	11,0	0,7	14,5	0,4	37,1	0,5	14,3	0,4
1 to 3	Cu(K), Ga(K), In(L), S(K), Se(L)	16,9	0,6	5,0	0,8	17,9	0,4	39,9	0,5	20,4	0,3
	Cu(L), Ga(L), In(L), S(K), Se(L)	23,6	0,5	11,0	0,7	14,2	0,3	32,8	0,4	18,4	0,3
1 to 5	Cu(K), Ga(K), In(L), S(K), Se(L)	19,7	0,7	4,6	0,8	20,5	0,4	35,6	0,4	19,5	0,3
	Cu(L), Ga(L), In(L), S(K), Se(L)	23,8	0,6	7,8	0,7	18,1	0,4	32,0	0,4	18,4	0,3
only 2	Cu(K), In(L), S(K), Se(L)	22,3	1,3	-	-	24,7	0,8	31,8	0,8	21,2	0,5
	Cu(L), In(L), S(K), Se(L)	25,4	0,9	-	-	23,5	0,8	30,4	0,7	20,7	0,5

**Table S2.** EDX data (at.%) for the ZnS-passivated particles obtained with a precursor ratio (**2** to **1+2**) of 0.67; fraction of small particles (compare Figure 5h in the article).

EDX line analysis	Cu	error	Ga	error	In	error	S	error	Se	error	Zn	error
Cu(K), Ga(K), In(L), S(K), Se(L), Zn(K)	10,3	0,8	3,1	0,5	13,2	0,5	51,3	0,6	14,4	0,4	7,8	0,9
Cu(L), Ga(L), In(L), S(K), Se(L), Zn(L)	16,4	0,4	8,2	0,5	8,7	0,3	36,8	0,4	12,2	0,3	17,7	0,4
Cu(K), Ga(K), In(L), S(K), Se(L), Zn(K)	11,3	0,5	3,3	0,4	12,6	0,4	50,4	0,4	13,1	0,2	9,4	0,6
Cu(L), Ga(L), In(L), S(K), Se(L), Zn(L)	15,0	0,3	6,9	0,4	9,6	0,3	40,4	0,3	11,7	0,2	16,5	0,3
average value	13,2		5,3		11,0		44,7		12,8		12,8	

**Table S3.** EDX data (at.%) for the ZnS-passivated particles obtained with a precursor ratio (**2** to **1+2**) of 0.67; fraction of large particles (compare Figure 5g in the article).

EDX line analysis	Cu	error	Ga	error	In	error	S	error	Se	error	Zn	error
Cu(K), Ga(K), In(L), S(K), Se(L), Zn(K)	8,6	0,6	2,6	0,4	12,5	0,5	57,7	0,6	14,2	0,3	4,5	0,4
Cu(L), Ga(L), In(L), S(K), Se(L), Zn(L)	18,4	0,3	11,9	0,4	6,9	0,3	36,2	0,4	11,4	0,3	15,2	0,3
Cu(K), Ga(K), In(L), S(K), Se(L), Zn(K)	7,2	0,5	1,3	0,3	14,2	0,4	59,3	0,5	15,6	0,2	2,5	0,3
Cu(L), Ga(L), In(L), S(K), Se(L), Zn(L)	20,2	0,3	12,2	0,3	7,7	0,2	36,4	0,3	12,6	0,2	11,0	0,4
average	13,6		7,0		10,3		47,4		13,4		8,3	

### Powder X-ray diffraction

Rietveld fits were applied to the powder patterns in order to obtain the lattice constants of the nanocrystals. The General Structure Analysis System (GSAS)<sup>4</sup> has been used for this purpose. The sphalerite and wurtzite crystal structures have been substituted by Ga and In at the Zn position and partially Se at the S position, respectively. Due to the very broad reflections only the gaussian broadening parameter (GP) has been refined to model the peak shape. Peak asymmetry parameters (S/L and H/L) were calculated from the actual diffractometer geometry. The background has been modelled with a Chebyschev polynomial (GSAS background function 1), and the zero point of the diffractometer has been refined in addition to the lattice constant.

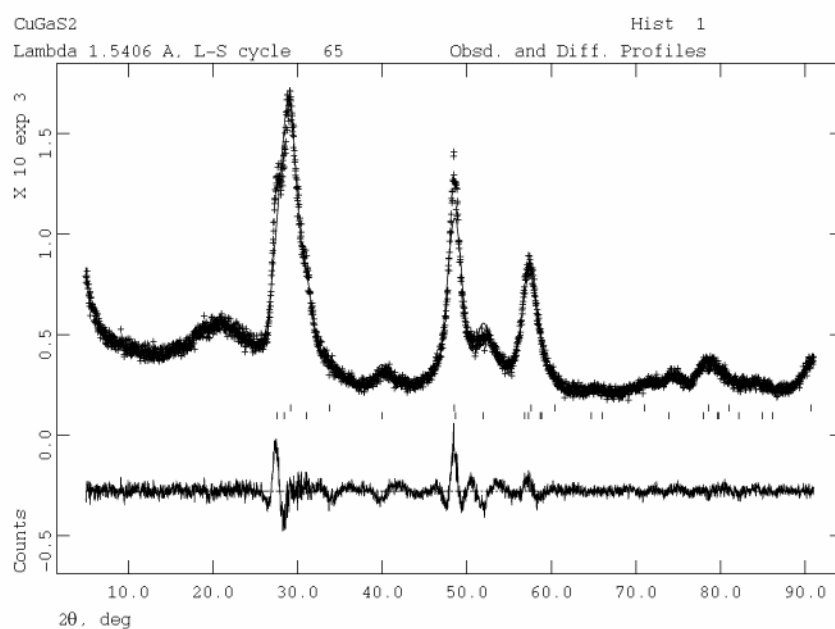


**Figure S5.** Rietveld fit ( $wR_p = 0.0733$ ,  $R_p = 0.0567$ ,  $R(F^2) = 0.0345$ ) of the powder pattern of the nanocrystal sample obtained from precursor **1** only. The observed (+) and calculated profile, reflection positions for cubic (first row,  $a = 530.6(3)$  pm) and hexagonal (second row,  $a = 374.1(2)$  pm,  $c = 629.0(5)$  pm) CuGaS<sub>2</sub> and the difference curve are displayed.

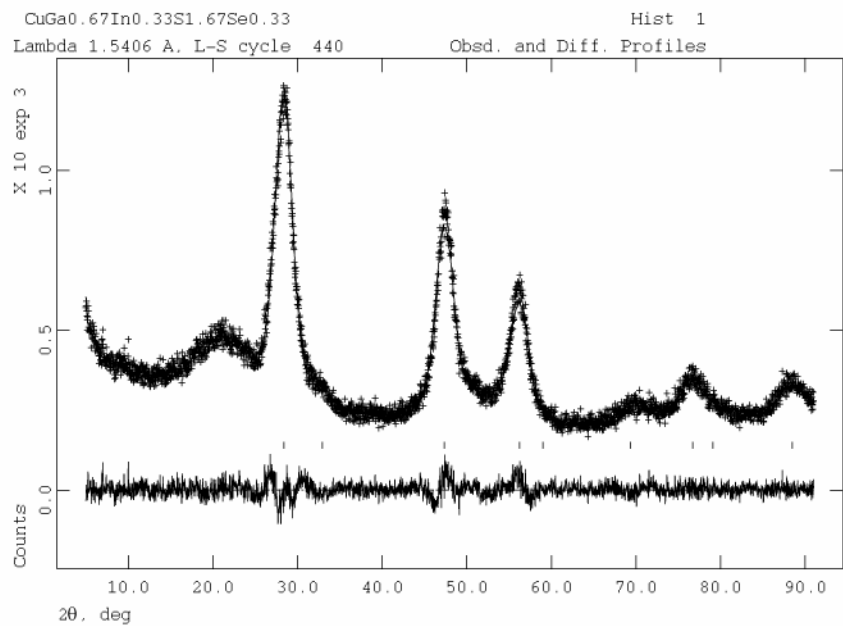


**Figure S6.** Rietveld fit ( $wR_p = 0.0593$ ,  $R_p = 0.0477$ ,  $R(F^2) = 0.0287$ ) of the powder pattern of the nanocrystal sample obtained from precursor **1** and **2** in a ratio of 2:1. The observed (+) and calculated profile, reflection positions for cubic ( $a = 539.8(2)$  pm)  $\text{CuGa}_{0.67}\text{In}_{0.33}\text{S}_{1.67}\text{Se}_{0.33}$  and the difference curve are displayed.

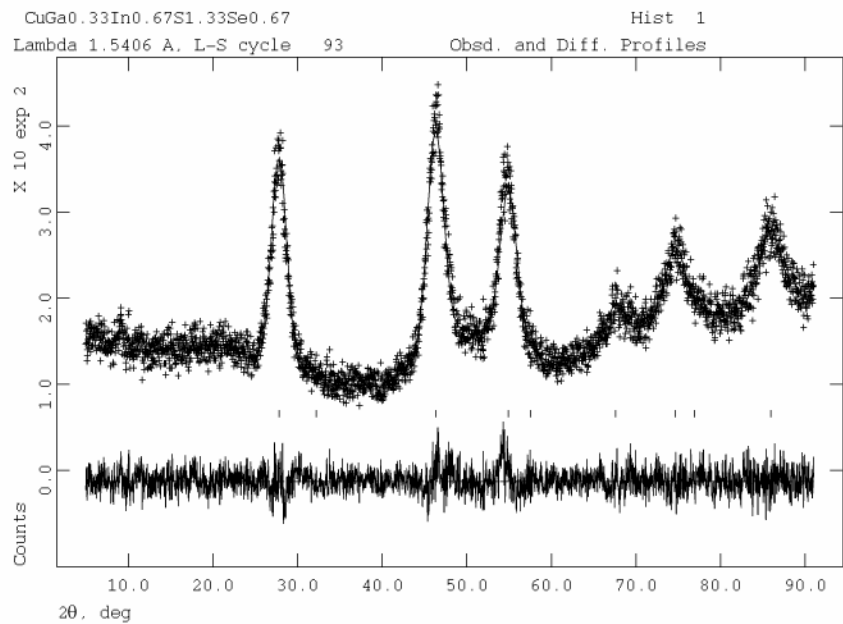


**Figure S7.** Rietveld fit ( $wR_p = 0.0795$ ,  $R_p = 0.0634$ ,  $R(F^2) = 0.0480$ ) of the powder pattern of the nanocrystal sample obtained from precursor **1** and **2** in a ratio of 1:2. The observed (+) and calculated profile, reflection positions for cubic ( $a = 553.1(3)$  pm)  $\text{CuGa}_{0.33}\text{In}_{0.67}\text{S}_{1.33}\text{Se}_{0.67}$  and the difference curve are displayed.

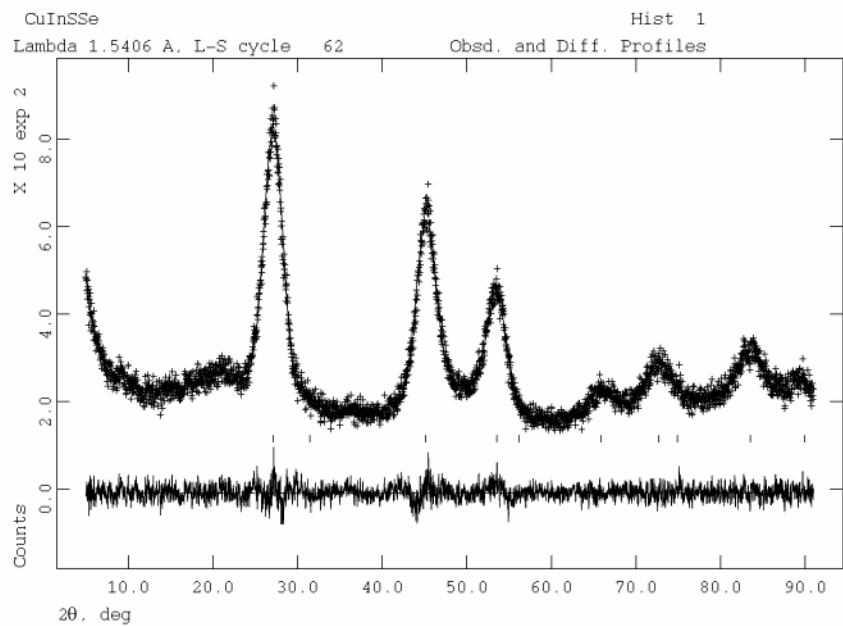


**Figure S8.** Rietveld fit ( $wR_p = 0.0651$ ,  $R_p = 0.0518$ ,  $R(F^2) = 0.0236$ ) of the powder pattern of the nanocrystal sample obtained from precursor **2** only. The observed (+) and calculated profile, reflection positions for cubic ( $a = 566.0(3)$  pm) CuInSSe and the difference curve are displayed.

### PL spectroscopy

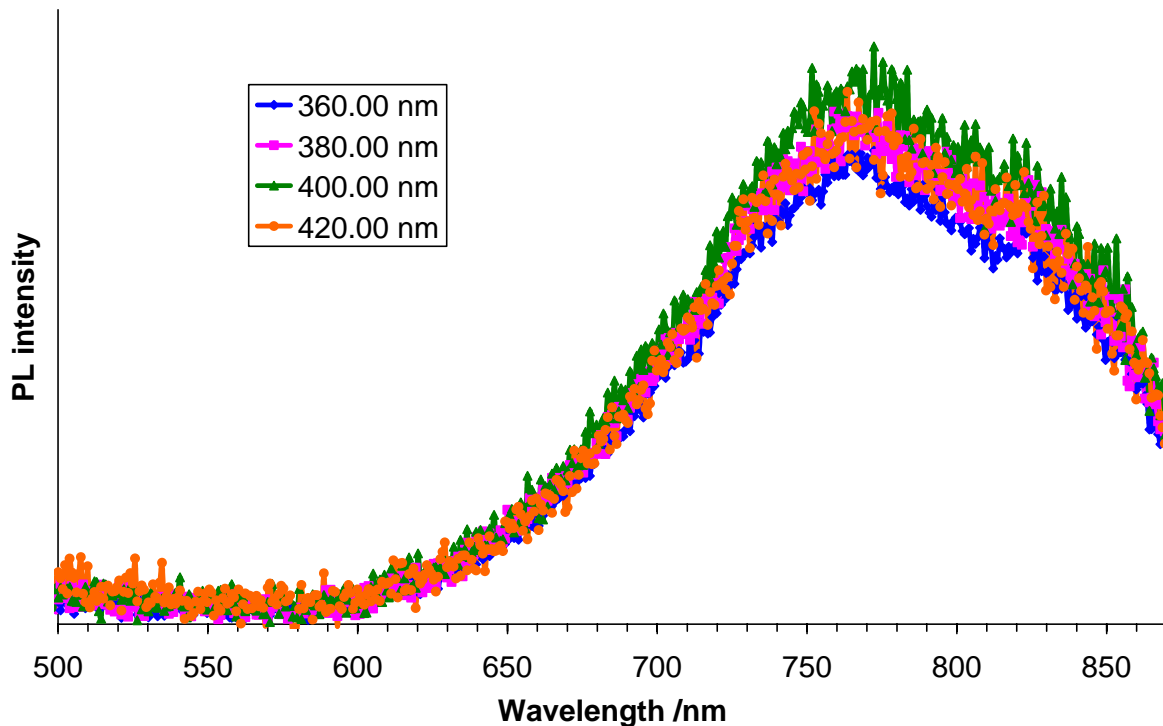


**Figure S9.** PL spectra of ZnS-passivated particles obtained with a precursor ratio (**2** to **1+2**) of 0.67. The spectra were recorded at different excitation wavelengths on the device used for quantum yield determination. Note the absence of the intensity decline around 690 nm.

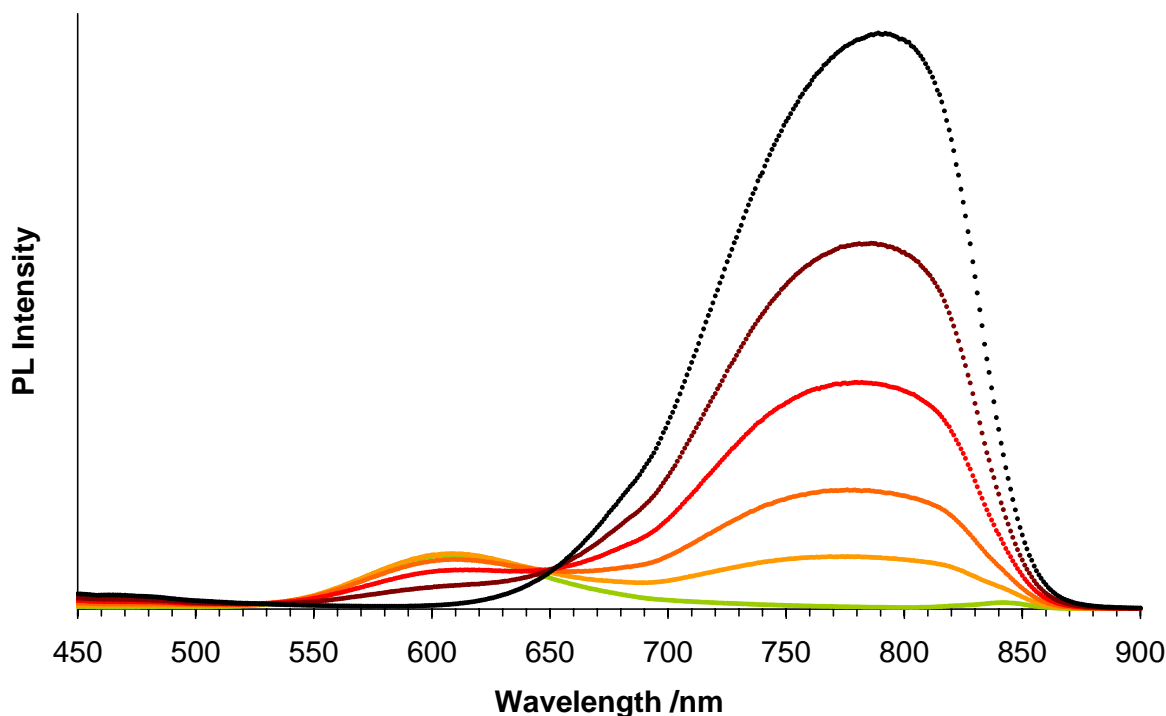


**Figure S10.** PL spectra of mixtures of ZnS-passivated particles obtained from either precursor **1** or **2**, respectively (*i.e.* mixtures of CuGaS<sub>2</sub> particles and CuIn(S,Se)<sub>2</sub> particles). Line colour code: from orange over red to black the concentration of the particles obtained from **2** increases. Note that these spectra do not resemble the spectra of the particles obtained from the co-thermolysis of **1** and **2** (compare Figure 3 in the manuscript), confirming their quasi-quinary composition.

## References

1. O. Kluge, R. Biedermann, J. Holldorf, H. Krautscheid, Organo Gallium / Indium Chalcogenide Complexes of Copper(I): Molecular Structures and Thermal Decomposition to Ternary Semiconductors. *Chem. Eur. J.* **2014**, *20*, 1318–1331.
2. O. Kluge, D. Friedrich, G. Wagner, H. Krautscheid, New organometallic single-source precursors for CuGaS<sub>2</sub> – polytypism in gallite nanocrystals obtained by thermolysis. *Dalton Trans.* **2012**, *42*, 8635–8642.
3. Q. Li, C. Zou, L. Zhai, J. Shen, L. Zhang, H. Yu, Y. Yang, X. Chen, S. Huang, Growth of wurtzite CuGaS<sub>2</sub> nanoribbons and their photoelectrical properties. *J. Alloys Compounds* **2013**, *567*, 127–133.
4. A. C. Larson, R. B. Von Dreele, *General Structure Analysis System (GSAS)*, Los Alamos National Laboratory Report LAUR 86-748 (2004).